Enhancement of thermal characteristics of a novel stearic acid-adipic acid eutectic phase change material integrated with expanded graphite for thermal energy storage applications

Kai Fu[a], Songping Mo[a,b,*], Zicong Zhou[a], Qing Li[a], Lisi Jia[a,b], Yanping Du[c], Ying Chen[a,b]

[a] *School of Materials and Energy, Guangdong University of Technology, Guangzhou 510006, China.*

[b] *Guangdong Provincial Key Laboratory on Functional Soft Condensed Matter, Guangdong University of Technology, Guangzhou 510006, China.*

[c] *School of Engineering, Lancaster University, Lancaster LA1 4YW, UK*

Abstract The utilization of phase change materials (PCMs) exhibiting exceptional thermal properties holds great significance for the advancement of sustainable energy utilization systems. Consequently, this research delves into the exploration of an innovative composite PCM formulated from a blend of stearic acid-adipic acid (SA-ADA) and expanded graphite (EG), with the SA-ADA component constituting 91% of the total mass. Through rigorous analysis, the microstructural, chemical and crystallographic characteristics of the composite were confirmed, revealing a uniform distribution of SA-ADA within the porous EG matrix, indicative of their exceptional compatibility without any discernible chemical interaction. Notably, the SA-ADA/EG composite exhibited a melting point of 65.7 °C and a latent heat of 185.3 kJ/kg, indicating its remarkable thermal performance. Furthermore, the thermal conductivity of this composite was significantly enhanced, achieving 8.375 $W \cdot m^{-1} \cdot K^{-1}$, which represents a remarkable 27.7-fold improvement over that of pure SA-ADA. This enhancement translated into substantial reductions in charging and discharging durations by 65.7% and 32.7%, respectively. Thermogravimetric analysis revealed that the thermal decomposition threshold far exceeded the phase change temperature, demonstrating robust thermal stability of the composite. Additionally, after enduring 500 thermal cycles, the composite demonstrated exceptional cycling stability. These

*Corresponding author.

E-mail address: mosp@ustc.edu.

findings suggest the great potential of SA-ADA/EG composite PCMs as promising candidates for thermal storage applications.

Keywords: Thermal energy storage, Phase change material, Eutectic, Expanded graphite, Adipic acid, Stearic acid

1. Introduction

Renewable energy has gained significant attention as a potential solution to rising greenhouse gas emissions and dwindling fossil fuel resources. However, the intermittent nature of renewable energy sources necessitates the development of effective energy storage technologies [1]. Thermal energy storage (TES) is as a promising solution to address temporal, spatial, and intensity discrepancies in renewable energy applications. The main categories of TES methods include sensible heat storage (SHS) [2], latent heat storage (LHS) [3] and thermochemical storage (TCHS) [4]. Among these, LHS has garnered the most interest due to its high energy storage density and safety features [5]. Phase change materials (PCMs) are commonly utilized for LHS, leveraging the latent heat charged and discharged during phase changes to store energy. PCM-based energy storage offers stable temperature control, high energy density, and economic viability, making it suitable for applications [6], such as solar thermal storage [7], electronic cooling [8, 9], cold chain logistics [10], and building energy conservation [11]. These materials hold immense potential for various energy storage applications [12].

PCMs can be categorized into organic, inorganic, and eutectic PCMs according to on their chemical properties [13, 14]. Inorganic PCMs consist of molten salts, hydrated salts, metals, and alloys [15]. Despite having a higher thermal conductivity, inorganic phase change materials face challenges such as high supercooling, phase separation, corrosion susceptibility, and poor stability [16]. On the other hand, organic phase change materials such as paraffin, and polyethylene glycol [17], offer advantages including high latent heat of phase change and minimal supercooling, attracting considerable interest in medium and low temperature TES research [18, 19].

To broaden their applications, eutectic organic PCMs have been proposed by

blending multiple organic PCMs together [20, 21]. Innovative studies by researchers have contributed to the development of eutectic phase change materials with desirable properties for TES applications. For instance, Kumar et al. [22] conducted research on the phase diagram of binary mixtures of lauric acid (LA), myristic acid (MA), palmitic acid (PA) and 1-dodecanol (DE). Jacob et al. [23] employed a melt blending technique to produce a binary eutectic PCM (BEPCM) by combining paraffin wax and palmitic acid. This process resulted in enhanced thermal conductivity and latent heat values, making it ideal for medium-temperature TES applications.

Organic PCMs face limitations such as low thermal conductivity, poor thermal durability, and easily leakage, all of which impede their phase change performance [24]. To resolve this issue, researchers integrate PCMs with porous matrices to create shape-stable composite PCMs [25]. Various types of support materials, including metal-based, carbon-based, polymer-based, bio-based, and clay mineral-based nanostructure materials, are utilized for shape stabilization [26]. Porous materials have been found to be effective in maintaining PCMs within their pores to prevent leakage [27]. Expanded graphite (EG) has become a favored porous matrix material owing to its excellent thermal conductivity, numerous nanopores, low density, strong compatibility with PCMs [28, 29], and convenient fabrication [30]. Studies by Wang et al. [31], Yang et al. [32] and Yan et al. [33] have demonstrated the effectiveness of incorporating EG into composite phase change materials, leading to enhanced thermal conductivity and decreased supercooling. Additionally, research by Yu et al. [34] has successfully prepared paraffin/EG composite PCMs that exhibit minimal leakage, even after multiple melting and solidification cycles.

Dicarboxylic acids (DAs) are regarded as promising organic phase change materials (PCMs) due to their high latent heat and low supercooling degree [35]. Natural dicarboxylic acids, such as adipic acid (ADA), have high latent heat values as well as low costs, making them ideal alternative for TES [36]. Other DAs, such as sebacic acid (SEA) [37] and azelaic acid (AA) [38], have high latent heat and low supercooling, but have higher phase change temperatures, limiting their applicability in low-temperature TES systems.

Furthermore, DAs are susceptible to thermal decomposition at temperatures above their melting points [39, 40], limiting their long-term stability and thermal cycling performance in high-temperature environments. Eutectic technology effectively adjusts PCM melting points, making them better suited for use in TES systems. Eutectic technology entails combining two or more PCMs to obtain the attainable melting point, considerably simplifying the work of matching PCM [40].

This study presents a binary eutectic PCM made up of stearic acid (SA) and ADA. Stearic acid has gained popularity because of its high latent heat and high stability, which compensate for the limitations of adipic acid. However, the incorporation of SA-ADA into EG has not been studied. In this study, SA-ADA/EG composite PCMs were prepared for the first time through physical impregnation approach to increase thermal performance and thermal cycling stability. Experiments were carried out to optimize the EG content. A thorough analysis of the morphology, chemical and crystal structure, phase change characteristics, thermal characteristics, charge and discharge capabilities, and thermal durability of the composites showed how promising these novel composites are for use in TES applications.

2. Experimental

2.1 Materials

Stearic acid (98%, chemical reagent), adipic acid (98%, chemical reagent) were purchased from Shanghai McLean Biochemical Technology Co. Ltd., China. Expanded graphite (10 mesh, expanded 200-300 times) was sourced from Nanjing Geruifa Carbon Materials Co. Ltd., China. The chemicals were used as received, without any additional purification. The properties of the pure PCMs are shown in Table 1.

Table 1 Properties of SA and ADA.

PCM	Molecular weight (g/mol)	Appearance	T_m (℃)	H_m (kJ/kg)
Stearic acid	284.48	White particles	68.4	208
Adipic acid	146.14	White powder	151.0	250

2.2 Preparation of SA–ADA eutectic mixture

Based on the well-established principles of phase equilibrium theory and thermodynamics, it is feasible to theoretically predict the optimal ratio of binary eutectic organic PCMs composed of SA and ADA, as reported in [41]. The melting temperature (T_m) and melting enthalpy (H_m) of this eutectic mixture can be calculated by equations (1) and (2), respectively.

$$1/T_m = 1/T_i - Rlnx_i/H_i \quad (1)$$

$$H_m = T_m \sum_{i=1}^{n}(X_i H_i/T_i) \quad (2)$$

According to the reference, the optimal mass ratio of SA to ADA in the binary eutectic mixture resulting in the highest latent heat is 25:1 [42]. An electronic balance was used to precisely measure the amount of SA and ADA, which were then transferred to the same clean beaker. The beaker was put in the center of a magnetic stirrer set to 150 °C ± 5 °C. The beaker was heated in an oil bath until the sample inside had completely melted into liquid. The magnetic stirrer was set to 500 rpm. The mixture in the beaker was stirred with a magnetic stirrer for around 30 min to ensure that the SA and ADA were thoroughly mixed.

2.3 Preparation of SA-ADA/EG

A series of SA-ADA/EG composites were prepared using the melt-blending method, with the SA-ADA eutectic mixture serving as the PCM and EG serving dual roles as both the matrix material and thermal conductivity enhancer. As shown in Fig. 1, 1.82 g, 2.34 g, and 2.86 g of EG were weighed and added to the molten eutectic mixture at mass percentages of 7 wt%, 9 wt%, and 11 wt%, respectively, based on the total mass of 26.00 g for each set of PCMs. Subsequently, the mixture was mechanically stirred for one hour to guarantee full adsorption into the EG. After cooling to room temperature, the SA-ADA/EG composites was successfully produced.

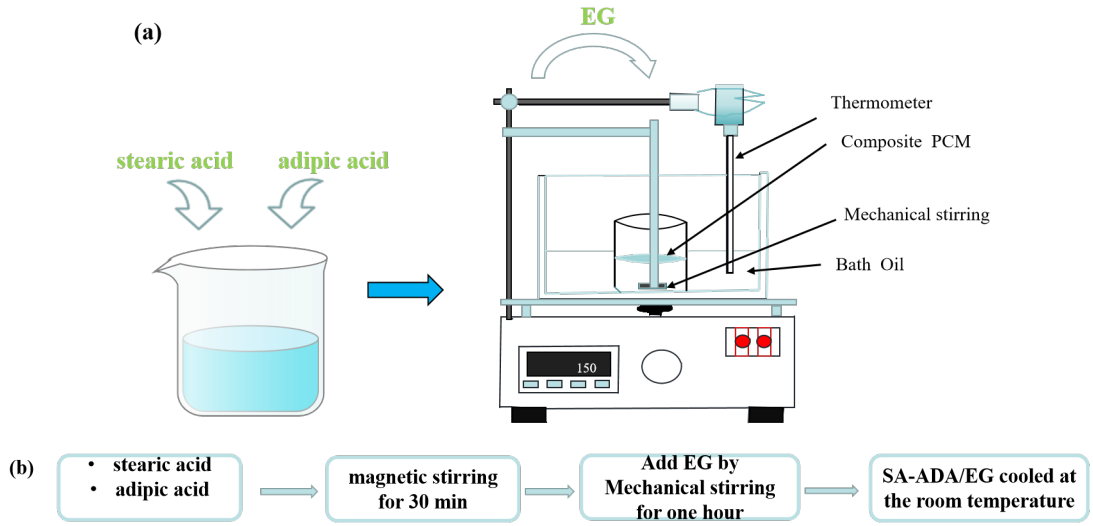

Fig. 1 Schematic of the (a) device and (b) procedure for preparation of SA-ADA/EG

2.4 Characterization of SA-ADA/EG

The morphology and microstructure of EG and SA-ADA/EG composite were examined utilizing a field emission scanning electron microscope (SEM, SU8010, Hitachi Inc., Japan). Differential scanning calorimetry (DSC DSC3 STAR, Mettler Toledo, Switzerland) was employed to analyze the phase change behavior of SA-ADA and SA-ADA/EG in a nitrogen atmosphere, with heating and cooling rates of 10 °C/min within 30-100 °C. Fourier transform infrared spectroscopy (FTIR, Nicolet 6700, Thermo Fisher Scientific, America) was utilized to investigate the chemical structure of SA-ADA, EG, and SA-ADA/EG, with results recorded in 4000-400 cm^{-1}. In-situ X-ray diffractometry (XRD, Ultima IV X, Rigaku Corporation, Japan) was conducted to characterize the crystal structure of the materials. Thermal conductivity was measure utilizing a precision thermal constant analyzer, model TPS 500 S, manufactured by Hot Disk Inc., Sweden. The transient plane source technique was adopted for these measurements, which necessitates the placement of two circular samples of the test material, possessing comparable thicknesses, in direct contact with the probe. Subsequently, these samples were heated at a fixed power level for a predefined scan duration. The selection of probe type, heating power, and scan time for these tests was guided by factors such as the diameter, thickness, and anticipated thermal conductivity range of each individual sample. Thermogravimetric analysis (TGA, SDT Q600) was performed to study the thermal stability under 20 °C/min in 25-600 °C. A thermal

cycling chamber was used to accomplish up to 200 repeated melting and solidification cycles. The test cycled between temperatures of 50 °C and 80 °C. DSC was then used to examine the changes caused by the thermal cycling.

The heat charging and discharging performance of SA-ADA/EG were evaluated to assess the impact of EG on the performance of the SA-ADA. Fig. 2 depicts the experimental setup. The apparatus comprises an Agilent data acquisition instrument （34901A, Malaysia）, a thermocouple, a computer, and a water bath. Initially, a 5-gram sample was placed in a 120 ml test tube. A thermocouple was then inserted into the center of the test tube, encased by the sample, to ensure precise temperature measurements. Then place the test tube in a water bath at 75 °C and continue to heat it. Once the temperature reached the preset target, the sample was removed from the bath and allowed to cool naturally. This process allows for the tracking of the temperature changes within the sample during both heating and cooling. The Agilent data logger facilitates this by recording temperature variations every 10 s, ensuring an accurate dataset for subsequent analysis. Table 2 summarizes the accuracy of the main devices.

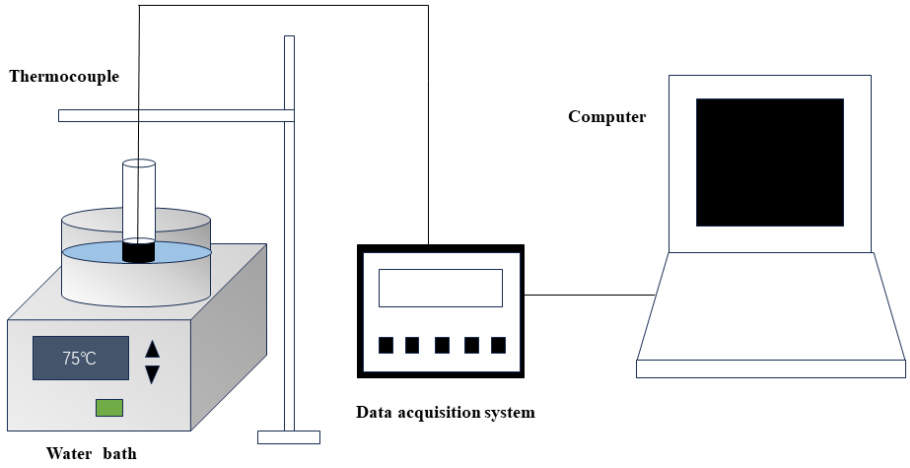

Fig. 2 Schematic of the setup for thermal performance measurement

Table 2 Accuracy of the devices

Device	Measured parameter	Accuracy
DSC	Enthalpy	±3%
Thermal constant analyzer	Thermal conductivity	±5%
BTH-80B test chamber	Thermal reliability	±0.5°C
Thermogravimetric analyzer	Mass	0.001%
Thermocouple	Temperature	±1°C

3. Results and discussion

3.1 Optimization of mass ratio of SA-ADA to EG

The phase change temperature, latent heat, and thermal conductivity are crucial characteristics that determine the applicability of PCMs. A higher PCM content results in increased heat storage capacity. However, with a small of EG content, saturation of internal pore structures may occur, leading to leakage of excess PCM to the surface of EG. Therefore, optimizing the mass ratio of SA-ADA to EG is essential. To assess the shape stability of SA-ADA/EG, a leakage test was conducted by placing 0.2 g of SA-ADA/EG with varying EG contents (7wt%, 9wt%, 11wt%) on filter paper in a drying oven at 120 °C for 120 min, with photos taken before and after heating for comparison.

The adsorption of the melted PCM by the filter paper_and reflects the shape stability of the SA-ADA/EG. Fig. 3 presents the photographs of SA-ADA/EG prior to (a) and following (b) heat treatment. According to the comparison photos, it can be found that when the EG content in SA-ADA/EG is 9wt% and 11wt%, the sample has almost no leakage. When the EG content was 7wt%, obvious leakage was observed on the filter paper. This result indicates that EG could not adsorb more SA-ADA, and excess SA-ADA would be adsorbed on the EG surface and ooze out after heating. Therefore, in order to effectively prevent the efflux of SA-ADA from EG, the maximum mass fraction of SA-ADA in the composite is about 91%.

The initial mass of the sample is recorded as M_0, while the residual mass after heating for n hours is denoted as M_n. To determine the leakage rate (L_m) of each specimen after undergoing n hours of heating, the following formula is employed.

$$L_m(wt.\%) = (M_0 - M_n)/M_0 \times 100\% \quad (3)$$

To solidify this observation with quantitative data, the sample underwent precise weighing, and the change in mass ratio before and after heating, relative to its original mass, was calculated using the aforementioned formula. The results of this calculation are presented in Table 3, providing a clear understanding of the behavior of the sample under heating conditions. When the EG content in SA-ADA/EG is 7wt%, the mass ratio before and after heat treatment is lower than 90%. When the EG content exceeds 9 wt%, the post-heating to prior-heating mass ratio of the sample rapidly increases to more than

95 wt%, and it can be considered that there is basically no leakage. Based on visual assessments and quantitative measurements of mass loss, it was determined that SA-ADA/EG with an EG content of 9 wt% exhibited no leakage and was selected for further study.

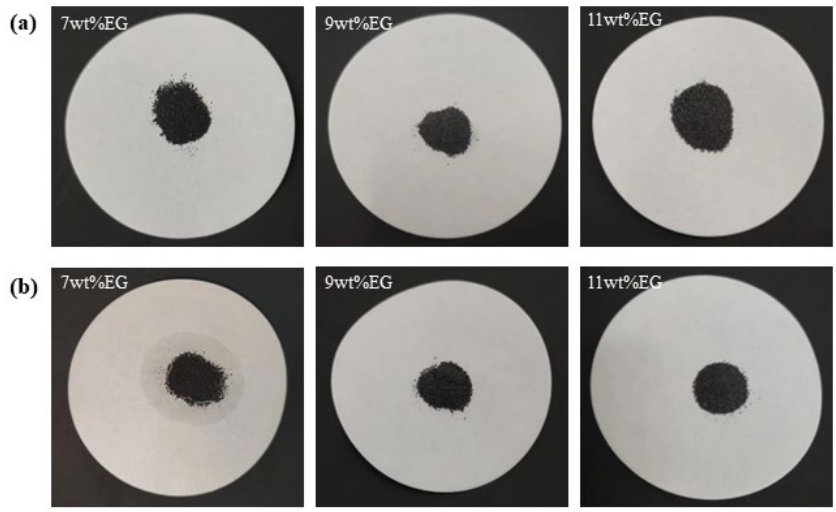

Fig. 3 Photographs of (a) prior- heating and (b) post-heating SA-ADA/EG.

Table 3 Weight of SA-ADA/EG before and after heat treatment

EG content (wt%)	Prior-heating (g)	Post-heating (g)	Percentage (%)
7	0.2	0.173	86.5
9	0.2	0.193	96.5
11	0.2	0.195	97.5

3.2 Morphology of SA–ADA/EG

Figure 4 shows the morphological characteristics of the samples. As illustrated in Fig. 4a, EG exhibits a layered structure composed of stacked graphite sheets, possessing a porous structure with significant porosity and a large specific surface area. These features enhance the adsorption capacity of EG, allowing it to effectively adsorb a high content of molten SA-ADA. In Fig. 4b, it is evident that the adsorption of the SA-ADA eutectic mixture results in a more smooth appearance of the EG sheets. The uniform distribution of SA-ADA within the pore structure of EG reveals great compatibility between SA-ADA and EG. Capillary force promotes the even distribution of SA-ADA within the pores of EG, effectively preventing the leakage of molten SA-ADA.

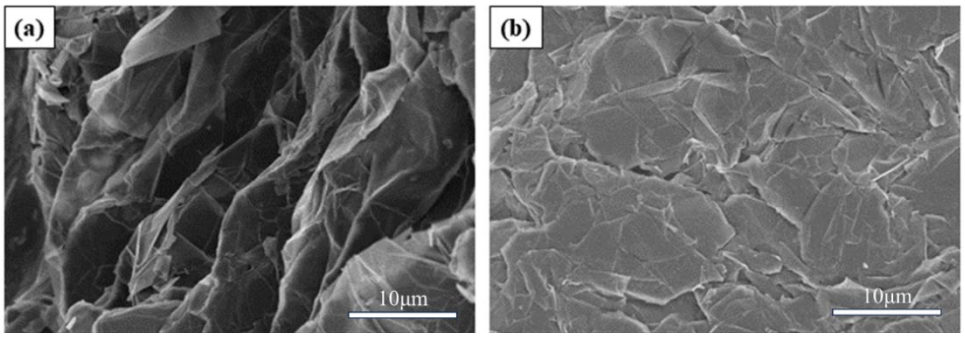

Fig. 4 SEM images of (a) EG and (b) SA-ADA/EG.

3.3 Chemical and crystal structure of SA–ADA/EG

The chemical synergy between SA-ADA and EG was explored using infrared spectroscopy, aiming to elucidate the nature of their interaction. Fig. 5 presents the Fourier-transform infrared (FT-IR) spectra for SA-ADA, EG, and the SA-ADA/EG blend .In the FT-IR spectrum of SA-ADA [42], the peaks located at 2919 cm^{-1} and 2854 cm^{-1} are respectively associated with the asymmetric and symmetric stretching vibrations of the $-CH_2$ group. The absorption peak observed at 1702.83 cm^{-1} is indicative of the stretching vibration of C=O group. Furthermore, the peak at 1463.7 cm^{-1} is linked to the $-CH_2$ group's bending vibration, while the one at 1292.07 cm^{-1} denotes the bending vibrations of both C-H and C-C bonds. Furthermore, the FT-IR spectrum of SA-ADA showcases a distinct absorption peak at 941.09 cm^{-1}, indicative of the out-of-plane rocking vibration of -OH group, with the in-plane bending vibration of C-H detected at 723.17 cm^{-1}. In the case of EG's infrared spectrum, notable peaks within the 3500 cm^{-1} to 1600 cm^{-1} range were identified. These are associated with the bending vibration of H-O-H, the antisymmetric stretching vibration of $-CH_2$, and EG's water absorption, influenced by atmospheric humidity during the analysis. [32, 43]. The composite SA-ADA/EG exhibited similar characteristic peaks as its individual components, these observations are mainly ascribed to the capillary force and surface tension exhibited by EG. When under pressure, these properties promote the diffusion of SA-ADA into the pores of EG, leading to a process of physical adsorption without the formation of new chemical bonds.

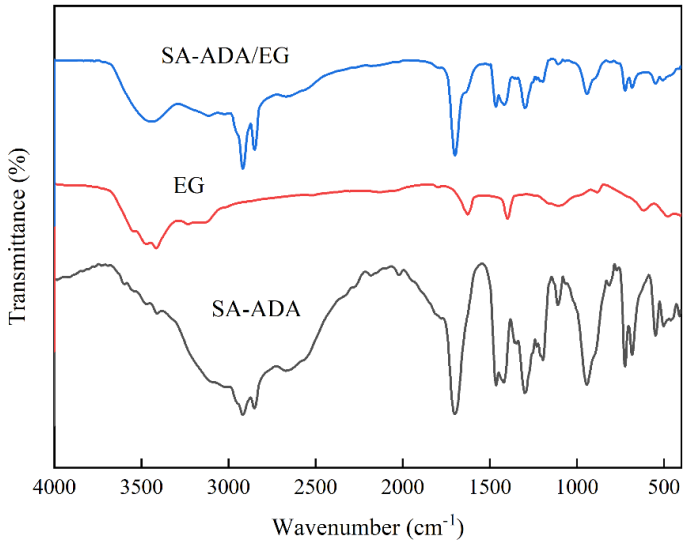

Fig. 5 FT-IR spectra of SA-ADA, EG and SA-ADA/EG.

X-ray diffraction analysis was carried out to examine the crystal structures of SA-ADA, EG, and SA-ADA/EG, as depicted in Fig. 6. The analysis identified a weak diffraction peak at 2θ=11.54°, and two prominent peaks at 2θ=22.02° and 2θ=24.58° for SA-ADA [44], and a strong peak at 2θ=26.64° was observed for EG. The XRD pattern of the SA-ADA/EG composite showed diffraction peaks from both SA-ADA and EG, with no new peaks emerging, indicating that the inclusion of EG did not modify the crystal structure of SA-ADA. This indicates that the prepared SA-ADA/EG maintained a stable chemical structure without significant changes.

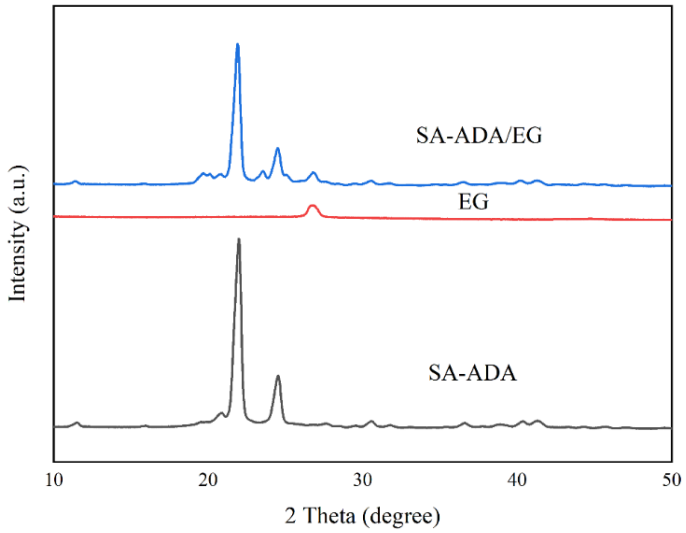

Fig. 6 XRD patterns of SA-ADA, EG and SA-ADA/EG.

3.4 Phase change characteristics of SA-ADA/EG

The DSC profiles depicted in Fig. 7 showcase the melting and solidification processes of SA-ADA and its composite, SA-ADA/EG. Both compounds display a distinct single peak, indicating a straightforward solid-liquid phase change without secondary peaks. The melting and solidification points for SA-ADA stand at 66.9°C and 64.2 °C, with corresponding latent heats of 205.0 kJ/kg and 204.0 kJ/kg. In contrast, SA-ADA/EG records melting and solidification temperatures of 65.7 °C and 66.6 °C, along with latent heats of 185.3 kJ/kg and 184.5 kJ/kg, respectively. The latent heat for phase changes within a composite material can be precisely determined by applying the latent heat of its components proportionate to their mass fraction in the mixture. Accordingly, the predicted latent heats for the melting and solidification of the SA-ADA/EG composite are 182.5 kJ/kg and 181.6 kJ/kg. When these theoretical predictions are compared with the experimental outcomes, the calculated latent heats closely match the measured values, showing a variance of less than 3%. The marginally reduced melting point of SA-ADA/EG relative to SA-ADA can be ascribed to the enhanced thermal conductivity of the supporting material, EG. The SA-ADA/EG composite has a lower latent heat than pure SA-ADA because EG remains inactive during the phase change of the PCM. This improvement accelerates heat distribution, thereby lowering the temperature required for melting [45]. Additionally, the pore structure of EG weakens inter-molecular forces between SA-ADA molecules within the confined EG pores [46], influencing the solidification temperature. This effect is further supported by the larger specific surface area of EG, providing nucleation sites for solidification and resulting in a higher solidification temperature [35].

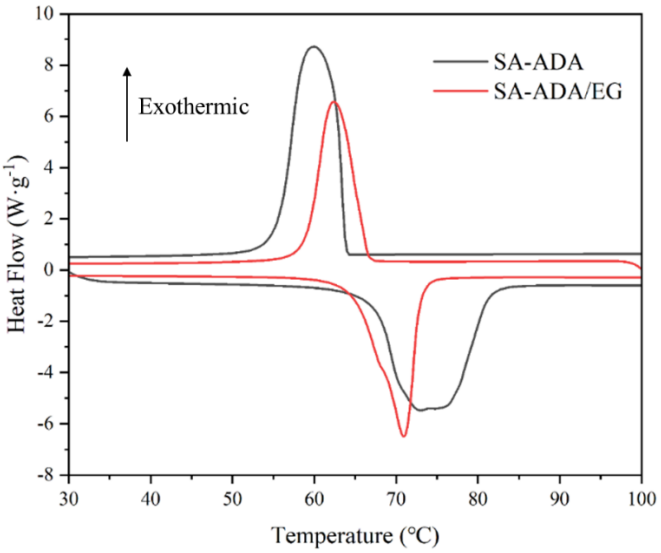

Fig. 7 DSC curves of SA-ADA and SA-ADA/EG.

The supercooling degree is the temperature difference between the melting point and the freezing (crystallization) point. It can be expressed by the following equation [47]:

$$\Delta T_s = T_m - T_f \quad (4)$$

where, ΔT_s represents the supercooling degree, T_m is the melting temperature, and T_f is the freezing temperature. The supercooling degree is derived using Eq. (4). The addition of EG reduces the supercooling degree from 2.7 °C for SA-ADA to -0.9 °C for SA-ADA/EG. SA-ADA/EG has a negative supercooling degree because, in this study, the melting and freezing temperatures refer to the onset temperature of melting and freezing, which is the intersection of the baseline and the tangent of the melting or freezing peak in the heat flow curve [48]. Negative supercooling degree values have also been recorded in the literature [43, 49]. The onset temperature was chosen as the phase change temperature because it is less impacted by sample mass and the pace of heating or cooling rate. The incorporation of EG results in structural transitions of the SA-ADA in the EG pores, resulting in changes in melting and solidification temperatures [50], a decrease in supercooling degree, and better phase change characteristics.

Table 4 presents a comparative analysis of the present results with those of other composite PCMs reported in prior literature. The SA-ADA/EG examined in the present study exhibits higher latent heat compared to the other stearic acid-based composite

PCMs. It is noteworthy that, in comparison to stearic acid/carbonized maize straw [51] and stearic acid/expanded graphite [52], which possess comparable phase change temperatures, the SA-ADA/EG exhibits a significantly higher latent heat. Consequently, the SA-ADA/EG possesses significant potential for TES applications in this temperature range.

Table 4 Comparison between SA-ADA/EG and composites reported in the literature

Sample	T_m(℃)	H_m(kJ/kg)	T_f(℃)	H_f(kJ/kg)	ΔT(℃)	Refs
Stearic acid/carbonized maize straw	67.62	160.74	65.28	160.47	2.34	[51]
Stearic acid/expanded graphite	67.96	163.35	67.08	163.29	0.88	[52]
Capric-Stearic Acid/Expanded Graphite	24.47	150.42	22.82	150.35	1.55	[18]
Lauric–myristic–palmitic acid ternary eutectic mixtures/expanded graphite	31.41	145.8	30.94	135.9	0.47	[45]
Lauric–myristic–stearic acid/expanded graphite	29.05	137.1	29.38	131.3	0.33	[53]
Palmitic-stearic acid eutectic mixture/expanded graphite	53.89	166.27	54.37	166.13	-0.57	[43]
SA-ADA/EG	65.7	185.3	66.6	184.5	-0.9	Present

3.5 Thermal conductivity and charging/discharging performance of SA-ADA/EG

Thermal conductivity is a vital parameter for PCMs in TES systems, significantly affecting their charging and discharging rates. This study utilizes the transient plane heat source method to evaluate the thermal conductivity of SA-ADA and various SA-ADA/EG composites with different EG mass fractions, as shown in Fig. 8. The thermal conductivity of SA-ADA, measured at room temperature, was recorded at 0.302 $W \cdot m^{-1} \cdot K^{-1}$, highlighting its inefficiency for TES. Conversely, increasing the EG content led to a nearly linear improvement in the thermal conductivity of the composite materials. Specifically, at EG concentrations of 7, 9, and 11 wt%, the thermal conductivity values were 6.679, 8.375, and 8.714 $W \cdot m^{-1} \cdot K^{-1}$, respectively. These values represent improvements of 22.1, 27.7, and 28.9 times that of SA-ADA, respectively. The results highlight the effectiveness of impregnating SA-ADA with EG in enhancing thermal conductivity. This enhancement is primarily due to the high thermal conductivity and

interconnected three-dimensional thermal conductive networks of EG within the composites [54, 55].

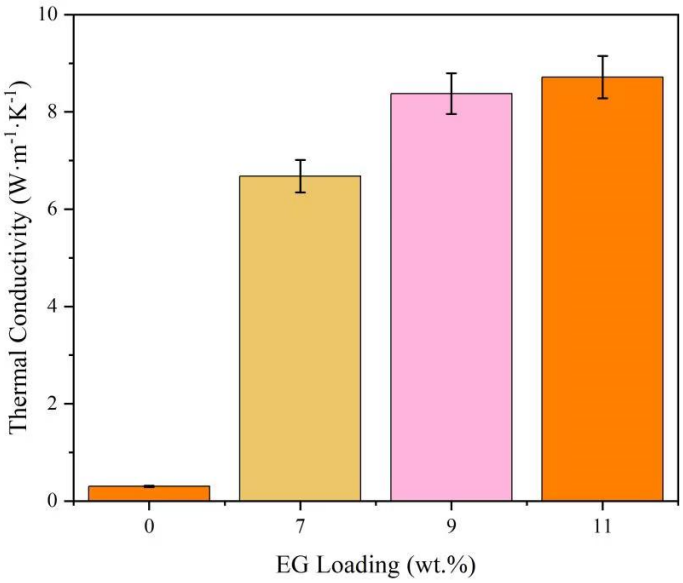

Fig. 8 Thermal conductivity of SA-ADA/EG with various mass fractions of EG.

A comprehensive comparison of this work with recent investigations on organic composite PCMs is presented in Table 5. Notably, SA-ADA/EG exhibits a superior thermal conductivity compared to previous results, emerging as a promising candidate for TES applications. This enhancement can be attributed to the exceptional compatibility between SA-ADA and EG, which effectively minimizes the contact thermal resistance between the two components.

Table 5 Comparison between SA-ADA/EG and composites in previous works

Sample	PCM content (wt%)	Thermal conductivity ($W \cdot m^{-1} \cdot K^{-1}$)	Ref.
Hexadecanol-palmitic acid/expanded graphite	85	3.483	[56]
Sodium acetate trihydrate-lithium chloride-potassium chloride/expanded graphite	86	4.54	[57]
Capric acid-stearic acid-octadecanol/ expanded graphite	91.67	3.236	[41]
Glutaric acid/expanded graphite	85	3.10	[58]
Octadecanoic acid/octadecanol/expanded graphite	91	3.38	[59]
SA-ADA/EG	91	8.375	Present

The temperature-time curves of thermal energy charging/discharging for both SA-ADA and SA-ADA/EG are illustrated in Fig. 9. As observed in Fig. 9a, the charging

process from 27 °C to 74 °C required 2500 s and 1050 s for SA-ADA and SA-ADA/EG, respectively. Moreover, the solid-liquid phase change for SA-ADA occurred between 60 °C and 66 °C, taking about 1050 seconds, whereas the SA-ADA/EG composite completed its phase change in a narrower temperature range of 60.5 °C to 64.3 °C in just 360 s. The discharging of SA-ADA from 74 °C to 27 °C took 1680 s, whereas SA-ADA/EG completed this process within 1300 s, as depicted in Fig. 9b. The SA-ADA completed solidification between 63.4 °C and 60.2 °C in roughly 550 seconds, while SA-ADA/EG achieved the same within the narrower range of 64 °C to 62.8 °C in about 370 seconds. Notably, the melting and solidification durations for SA-ADA/EG were reduced by 65.7% and 32.7%, respectively, compared to those of SA-ADA.

These findings demonstrate that EG notably boosts the thermal conductivity of the SA-ADA/EG composite, resulting in a marked decrease in charge/discharge durations compared to pure SA-ADA. As a result, the charge/discharge rates have been significantly enhanced.

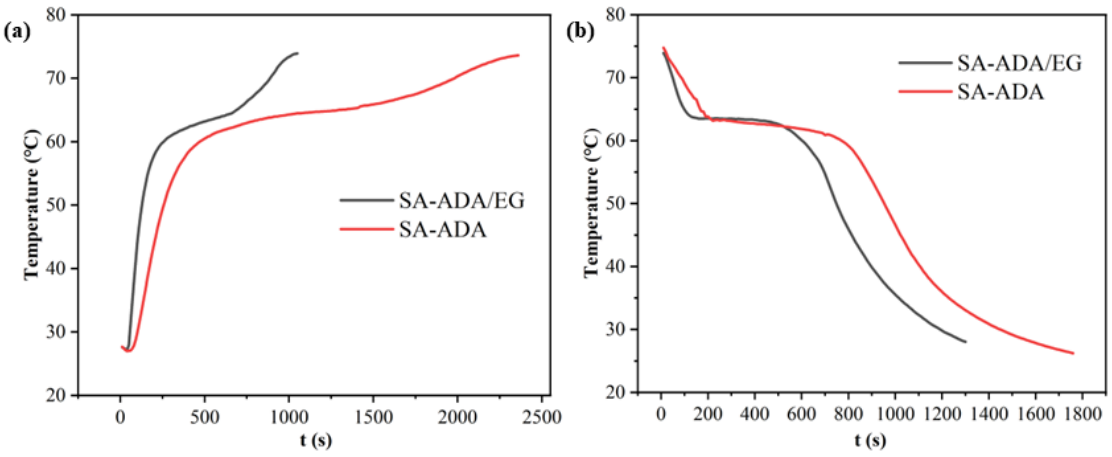

Fig. 9 Temperature-time curves of SA-ADA and SA-ADA/EG during charging and discharging.

3.6 Thermal stability and reliability of SA-ADA/EG

The weight loss profiles of SA-ADA, SA-ADA-EG, and EG were evaluated through thermogravimetric analysis from ambient temperature to 600 °C. The thermogravimetric curve depicted in Fig. 10 illustrates the negligible weight loss exhibited by EG within the temperature range, indicating its robust thermal stability. A comparison of the thermogravimetric curves of SA-ADA and SA-ADA/EG reveals that the onset temperature for weight loss in SA-ADA/EG is 185.7 °C, which is earlier than

that of SA-ADA, attributed to the enhanced thermal conductivity of EG, which leads to improved heat transfer within SA-ADA/EG. Furthermore, the onset decomposition temperature observed for SA-ADA/EG was more than 120 °C higher than its phase change temperature, demonstrating high thermal stability for its applications. With increasing temperature, the residual mass of both samples diminishes. Given the minimal weight loss exhibited by EG within this temperature range, the residual mass of the SA-ADA/EG composite primarily comprises of EG, with the residual mass closely aligning with the proportion of EG in the composite.

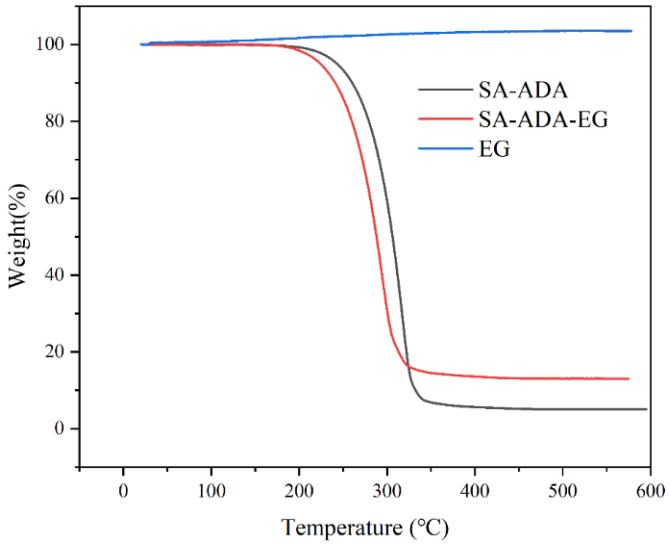

Fig. 10 Mass loss curves of SA-ADA, EG and SA-ADA/EG.

The performance of PCMs to consistently charge and discharge heat is referred to as thermal reliability. The thermal reliability of composites across numerous thermal cycles is of utmost importance for their practical applications. This reliability can be evaluated by monitoring the fluctuations in phase change temperature and latent heat that occur after multiple charging and discharging cycles. In the present study, the thermal stability was investigated through a series of thermal cycling experiments. As illustrated in Fig. 11, the DSC curves of SA-ADA/EG prior to and following 500 thermal cycles exhibit similar shapes, demonstrating consistent behavior throughout the endothermic and exothermic processes. Notably, both curves exhibit a single melting and solidification peak.

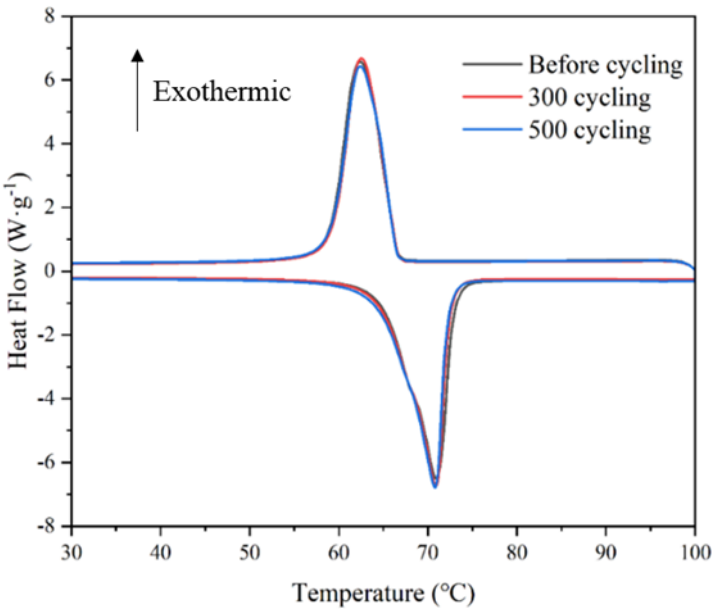

Fig. 11 DSC curves of SA-ADA/EG before and after thermal cycles.

A thorough thermal reliability assessment was conducted utilizing a thermal cycle chamber, where the sample was heated to 100 °C for 2 min and then cooled to 30 °C for 2 min. The temperature ramp rate was calibrated at 5 °C/min. Table 6 shows the results of an exhaustive analysis on the thermal performance of SA-ADA/EG after it has been subjected to 500 thermal cycles. Notably, the temperatures for both melting and solidification showed only trivial modifications, recording shifts of 0.8 °C and 0 °C, respectively, which suggest minimal variability. Additionally, there was a slight reduction in the latent heats of melting and solidification, with decreases of 5.9 kJ/kg and 6.2 kJ/kg, corresponding to minimal declines of 3.2% and 3.3%, respectively. The data further reveal that the disparities in phase change temperatures and latent heat values, recorded between the 300th and 500th cycles, were constrained to 0.2 °C and 0.1 kJ/kg, respectively. This highlights the exceptional thermal consistency of SA-ADA/EG.

Table 6 Phase change characteristics of SA-ADA/EG before and after thermal cycling.

Cycle	T_m(°C)	H_m(kJ/kg)	T_f(°C)	H_f(kJ/kg)
1	65.7	185.3	66.6	184.5
300	65.7	179.4	66.7	178.5
500	66.5	179.4	66.6	178.4

4. Conclusions

The preparation and comprehensive evaluation of an innovative shape-stable SA-ADA/EG composite PCM were presented in this study. The maximum adsorption capacity of SA-ADA by EG through physical adsorption was found to be 91%. The uniform distribution of SA-ADA within the pore structure of EG reveal great compatibility between SA-ADA and EG. The SA-ADA/EG composite exhibited melting and solidification temperatures at 65.7°C and 66.6°C, along with latent heats of 183.3 kJ/kg and 184.5 kJ/kg, respectively. Its thermal conductivity was enhanced by 27.7 times, achieving 8.375 $W \cdot m^{-1} \cdot K^{-1}$. The latent heat and thermal conductivity were higher than previous reported results. The durations for melting and solidification were reduced by 65.7% and 32.7%, respectively, when compared with the unmodified SA-ADA. The onset decomposition temperature of the composite was over 120 °C higher than its phase change temperature, demonstrating improved thermal stability. After 500 thermal cycles, the SA-ADA/EG maintained its phase change temperatures and latent heats with minimal change, demonstrating excellent thermal cycling stability. The results demonstrate that the SA-ADA/EG composite shows high latent heat, superior thermal conductivity, efficient charge/discharge behavior, robust thermal stability and thermal cycling stability across its functional temperature range. This positions it as an advantageous option for TES applications.

CRediT authorship contribution statement

Kai Fu: Investigation, Methodology, Writing-original draft. **Songping Mo**: Conceptualization, Funding acquisition, Project administration, Supervision, Writing-review & editing. **Zicong Zhou**: Investigation. **Qing Li**: Investigation. **Lisi Jia**: Writing-review & editing. **Yanping Du**: Writing-review & editing. **Ying Chen**: Resources.

Declaration of Competing Interests

The authors declare no competing financial interest.

Data availability

Data will be made available on request.

Acknowledgments

This work was supported by the National Natural Science Foundation of China (grant number 51976040).

References

[1] X Huang, X Chen, A Li, Shape-stabilized phase change materials based on porous supports for thermal energy storage applications, Chem. Eng. J. 356 (2019) 641-661.
[2] Y B Tao, Y-L He, A review of phase change material and performance enhancement method for latent heat storage system, Renew. Sust. Energ. Rev. 93 (2018) 245-259.
[3] B M Tripathi, S K Shukla, P K S Rathore, A comprehensive review on solar to thermal energy conversion and storage using phase change materials, J. Energy Storage. 72 (2023) 108280.
[4] G Simonsen, R Ravotti, P O'neill, Biobased phase change materials in energy storage and thermal management technologies, Renew. Sust. Energ. Rev. 184 (2023) 113546.
[5] C Zhao, J Yan, X Tian, Progress in thermal energy storage technologies for achieving carbon neutrality, Carbon Neutrality. 2 (1) (2023) 10.
[6] S Tan, X Zhang, Progress of research on phase change energy storage materials in their thermal conductivity, J. Energy Storage. 61 (2023) 106772.
[7] V Kapsalis, D Karamanis, Solar thermal energy storage and heat pumps with phase change materials, Appl. Therm. Eng. 99 (2016) 1212-1224.
[8] Y Tomizawa, K Sasaki, A Kuroda, Experimental and numerical study on phase change material (PCM) for thermal management of mobile devices, Appl. Therm. Eng. 98 (2016) 320-329.
[9] S R Akhil Krishnan, S Suresh, V C Midhun, Experimental investigation of nanoparticle enhanced polyol solid–solid phase change material aided heat sink with integrated heat pipe for electronic cooling application, Therm. Sci. Eng. Prog. 46 (2023) 102222.
[10] L Liu, X Zhang, X Xu, Development of low-temperature eutectic phase change material with expanded graphite for vaccine cold chain logistics, Renew. Energ. 179 (2021) 2348-2358.
[11] C Chen, X Wang, F Ma, Preparation and characterization of modified activated carbon-based shape stabilized eutectic phase change materials for gypsum composites application, Constr Build Mater. 369 (2023) 130551.
[12] Z-R Li, N Hu, L-W Fan, Nanocomposite phase change materials for high-performance thermal energy storage: A critical review, Energy Stor. Mater. 55 (2023) 727-753.
[13] V Jagadeeswara Reddy, K Akhila, P Dixit, Thermal buffering performance evaluation of fatty acids blend/fatty alcohol based eutectic phase change material and simulation, J. Energy Storage. 38 (2021) 102499.
[14] X Cui, P Liu, Z Tan, Preparation and thermal performance enhancement of roasted iron tailings based shape-stabilized phase change materials for thermal storage, Therm. Sci. Eng. Prog. 50 (2024) 102571.
[15] X Tang, B Zhu, M Xu, Shape-stabilized phase change materials based on fatty acid eutectics/expanded graphite composites for thermal storage, Energy Build. 109 (2015) 353-360.
[16] H Fauzi, H S C Metselaar, T M I Mahlia, Sodium laurate enhancements the thermal properties and thermal conductivity of eutectic fatty acid as phase change material (PCM), Sol Energy. 102 (2014) 333-337.
[17] W Du, H Fei, Y Pan, Development of capric acid-stearic acid-palmitic acid low-eutectic phase

change material with expanded graphite for thermal energy storage, Constr Build Mater. 320 (2022) 126309.
[18] S Liu, X Zhang, X Zhu, A Low-Temperature Phase Change Material Based on Capric-Stearic Acid/Expanded Graphite for Thermal Energy Storage, ACS Omega. 6 (28) (2021) 17988-17998.
[19] Y Ma, M Zou, W Chen, Nano‐Ag modified bio‐based shape‐stable phase change material for thermal energy storage, Int. J. Energy Res. 46 (15) (2022) 23056-23068.
[20] M Sun, T Liu, H Sha, A review on thermal energy storage with eutectic phase change materials: Fundamentals and applications, J. Energy Storage. 68 (2023) 107713.
[21] V Chinnasamy, S Appukuttan, Preparation and thermal properties of lauric acid/myristyl alcohol as a novel binary eutectic phase change material for indoor thermal comfort, Energy Storage. 1 (5) (2019) e80.
[22] R Kumar, S Vyas, A Dixit, Fatty acids/1-dodecanol binary eutectic phase change materials for low temperature solar thermal applications: Design, development and thermal analysis, Sol Energy. 155 (2017) 1373-1379.
[23] J Jacob, J Paul, A K Pandey, Analyzing long-term reliability and potential of organic eutectic Phase Change Material as thermal batteries, J. Energy Storage. 74 (2023) 109480.
[24] W Ren, L Cao, D Zhang, Composite phase change material based on reduced graphene oxide/expanded graphite aerogel with improved thermal properties and shape‐stability, Int. J. Energy Res. 44 (1) (2019) 242-256.
[25] K Luo, D Wu, Y Wang, Preparation and characterization of lauric acid-stearic acid/fumed silica/expanded graphite thermally conductive enhanced composites, J. Energy Storage. 73 (2023) 109151.
[26] H H Mert, PolyHIPE composite based-form stable phase change material for thermal energy storage, Int. J. Energy Res. 44 (8) (2020) 6583-6594.
[27] Y Zhang, Z Jia, A Moqeet Hai, Shape-stabilization micromechanisms of form-stable phase change materials-A review, Compos. Part A Appl. Sci. Manuf. 160 (2022) 107047.
[28] M a J Mazumder, B Salhi, A Sari, Effects of carbon-based fillers on thermal properties of fatty acids and their eutectics as phase change materials used for thermal energy storage: A Review, J. Energy Storage. 35 (2021) 102329.
[29] G Zhang, L Chen, W Lu, Production of ternary organic phase change material combined with expanded graphite and its application in cold chain transportation, Therm. Sci. Eng. Prog. 46 (2023) 102204.
[30] Z Wang, S Liu, G Ma, Preparation and properties of caprylic-nonanoic acid mixture/expanded graphite composite as phase change material for thermal energy storage, Int. J. Energy Res. 41 (15) (2017) 2555-2564.
[31] T Wang, Y Liu, R Meng, Thermal performance of galactitol/mannitol eutectic mixture/expanded graphite composite as phase change material for thermal energy harvesting, J. Energy Storage. 34 (2021) 101997.
[32] X Yang, Y Yuan, N Zhang, Preparation and properties of myristic–palmitic–stearic acid/expanded graphite composites as phase change materials for energy storage, Sol Energy. 99 (2014) 259-266.
[33] K Yan, L Qiu, Y Feng, Erythritol/expanded graphite form-stable phase change materials with excellent thermophysical properties, J. Energy Storage. 68 (2023) 107667.
[34] X K Yu, Y B Tao, Preparation and characterization of paraffin/expanded graphite composite

phase change materials with high thermal conductivity, Int. J. Heat Mass Transf. 198 (2022) 123433.
[35] S Liu, L Han, S Xie, A novel medium-temperature form-stable phase change material based on dicarboxylic acid eutectic mixture/expanded graphite composites, Sol Energy. 143 (2017) 22-30.
[36] A V Kolyado, S M Alenova, I K Garkushin, Phase diagram of a system of adipic, glutaric, and sebacic acids, Russ. J. Phys. Chem. A. 90 (6) (2016) 1293.
[37] S Wang, P Qin, X Fang, A novel sebacic acid/expanded graphite composite phase change material for solar thermal medium-temperature applications, Sol Energy. 99 (2014) 283-290.
[38] G T Nguyen, H S Hwang, J Lee, Azelaic Acid/Expanded Graphite Composites with High Latent Heat Storage Capacity and Thermal Conductivity at Medium Temperature, ACS Omega. 6 (12) (2021) 8469-8476.
[39] P Singh, R K Sharma, A K Ansu, A comprehensive review on development of eutectic organic phase change materials and their composites for low and medium range thermal energy storage applications, Sol. Energy Mater Sol. Cells. 223 (2021) 110955.
[40] J Dai, F Ma, C Sangiorgi, Assessment of high-enthalpy composite eutectic phase change materials efficiency in asphalt binders for cooling pavements, J. Clean. Prod. 442 (2024) 140999.
[41] H Fei, Q He, W Du, Structural characteristics and thermal performances of capric acid-stearic acid-octadecanol adsorbed into porous expanded graphite under vacuum condition, J. Energy Storage. 72 (2023) 108326.
[42] G Ma, J Sun, S Xie, Solid-liquid phase equilibria of stearic acid and dicarboxylic acids binary mixtures as low temperature thermal energy storage materials, J. Chem. Thermodyn. 120 (2018) 60-71.
[43] N Zhang, Y Yuan, Y Du, Preparation and properties of palmitic-stearic acid eutectic mixture/expanded graphite composite as phase change material for energy storage, Energy. 78 (2014) 950-956.
[44] G Govindaraja, S Duraipandi, S A, Development and characterization of a novel eutectic mixture with stearyl alcohol and adipic acid for hot air storage applications, J. Energy Storage. 61 (2023) 106708.
[45] N Zhang, Y Yuan, X Wang, Preparation and characterization of lauric–myristic–palmitic acid ternary eutectic mixtures/expanded graphite composite phase change material for thermal energy storage, Chem. Eng. J. 231 (2013) 214-219.
[46] T Xu, Q Chen, G Huang, Preparation and thermal energy storage properties of d-Mannitol/expanded graphite composite phase change material, Sol. Energy Mater Sol. Cells. 155 (2016) 141-146.
[47] A Safari, R Saidur, F A Sulaiman, A review on supercooling of Phase Change Materials in thermal energy storage systems, Renew. Sust. Energ. Rev. 70 (2017) 905.
[48] H Fatahi, J Claverie, S Poncet, Thermal Characterization of Phase Change Materials by Differential Scanning Calorimetry: A Review, Appl. Sci. 12 (23) (2022) 12019.
[49] M H Zahir, S A Mohamed, R Saidur, Supercooling of phase-change materials and the techniques used to mitigate the phenomenon, Appl. Energy. 240 (2019) 793.
[50] L Zhao, Q Yu, M Li, Preparation and thermal properties of low-temperature composite phase-change materials based on a binary eutectic mixture with expanded graphite: Effect of particle size and mass fraction, J. Energy Storage. 40 (2021) 102778.
[51] R Wen, Y Liu, C Yang, Enhanced thermal properties of stearic acid/carbonized maize straw composite phase change material for thermal energy storage in buildings, J. Energy Storage. 36

(2021) 102420.
[52] C Ao, S Yan, S Zhao, Stearic acid/expanded graphite composite phase change material with high thermal conductivity for thermal energy storage, Energy Rep. 8 (2022) 4834-4843.
[53] C Liu, Y Yuan, N Zhang, A novel PCM of lauric–myristic–stearic acid/expanded graphite composite for thermal energy storage, Mater. Lett. 120 (2014) 43-46.
[54] P Cheng, X Chen, H Gao, Different dimensional nanoadditives for thermal conductivity enhancement of phase change materials: Fundamentals and applications, Nano Energy. 85 (2021) 105948.
[55] X Lin, X Zhang, L Liu, Polymer/expanded graphite-based flexible phase change material with high thermal conductivity for battery thermal management, J. Clean. Prod. 331 (2022) 130014.
[56] T Xu, R He, G Fan, Hexadecanol-palmitic acid/expanded graphite eutectic composite phase change material and its application in photovoltaic panel, Sol. Energy Mater Sol. Cells. 273 (2024) 112934.
[57] X Man, H Lu, Q Xu, Preparation and thermal property enhancement of sodium acetate trihydrate-lithium chloride-potassium chloride expanded graphite composite phase change materials, Sol. Energy Mater Sol. Cells. 266 (2024) 112695.
[58] G T Nguyen, T N Ly, N T Tran, Glutaric acid/expanded graphite composites as highly efficient shape-stabilized phase change materials at medium-temperature, J. Energy Storage. 63 (2023) 107038.
[59] Z An, H J M Pea, X Du, Preparation and characteristics optimization of octadecanoic acid/octadecanol/expanded graphite based composite phase change materials for energy storage, J. Energy Storage. 55 (2022) 105598.